JUSTC

Article

http://justc.ustc.edu.cn

Received: January 24, 2022; Accepted: March 07, 2022

Multifunctional artificial nacre via biomimetic matrix-directed mineralization

Yu-Feng Meng[1], Bo Yang[1], Li-Bo Mao[2] ✉, and Shu-Hong Yu[1,2] ✉

[1]*Department of Chemistry, Institute of Biomimetic Materials & Chemistry, University of Science and Technology of China, Hefei 230026, China;*

[2]*Hefei National Laboratory for Physical Sciences at the Microscale, University of Science and Technology of China, Hefei 230026, China*

✉Correspondence: Li-Bo Mao, E-mail: maolb@ustc.edu.cn; Shu-Hong Yu, E-mail: shyu@ustc.edu.cn

Graphical abstract

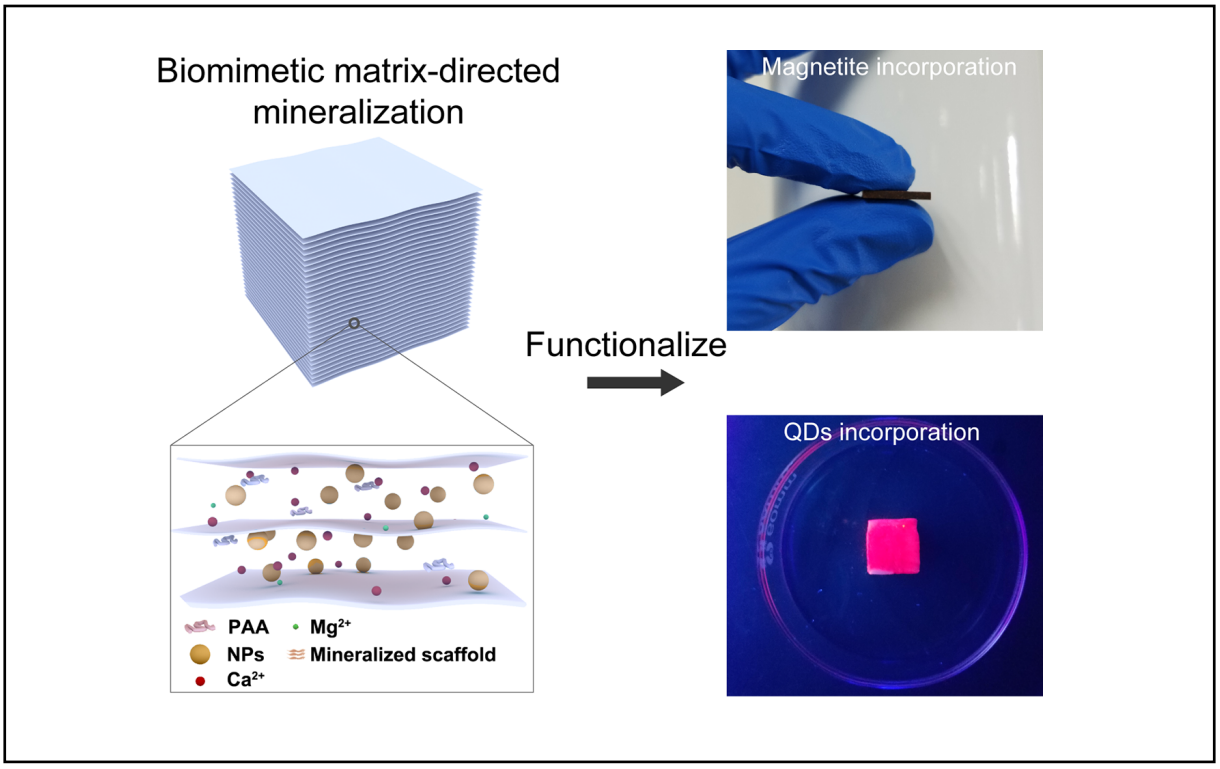

Artificial nacre with multiple functions and improved mechanical performance can be produced through a co-mineralization strategy.

Public summary

- Inspired by the in vivo growth of biological ceramics, a matrix-directed co-mineralization strategy is proposed to fabricate artificial nacre samples incorporated with different functional nanoparticles.
- The artificial nacre samples have similar functions as original nanoparticles, demonstrating their successful functionalization through the proposed strategy.
- By properly controlling the size and surface charge of the incorporated nanoparticles, the mechanical performance of the nanoparticle-incorporated artificial nacre samples can be significantly improved compared with that without nanoparticles.

Citation: Meng Y-F, Yang B, Mao L-B, et al. Multifunctional artificial nacre via biomimetic matrix-directed mineralization. *JUSTC*, **2022**, 52(7): 1. DOI: 10.52396/JUSTC-2022-0022

JUSTC

Article

http://justc.ustc.edu.cn

Received: January 24, 2022; Accepted: March 07, 2022

Multifunctional artificial nacre via biomimetic matrix-directed mineralization

Yu-Feng Meng[1], Bo Yang[1], Li-Bo Mao[2] ✉, and Shu-Hong Yu[1,2] ✉

[1]*Department of Chemistry, Institute of Biomimetic Materials & Chemistry, University of Science and Technology of China, Hefei 230026, China;*
[2]*Hefei National Laboratory for Physical Sciences at the Microscale, University of Science and Technology of China, Hefei 230026, China*

✉Correspondence: Li-Bo Mao, E-mail: maolb@ustc.edu.cn; Shu-Hong Yu, E-mail: shyu@ustc.edu.cn

Cite This: *JUSTC*, **2022**, 52(7): 1 (7pp)

Read Online

Abstract: Natural nacre, one of the most studied biological structural materials with delicate hierarchical structures and extraordinary performance, has inspired the design and fabrication of artificial structural ceramics with high fracture toughness. However, to meet the diverse requirements of different applications, future structural materials must be multifunctional with superior mechanical properties, such as strength, hardness, and toughness. Herein, based on the matrix-directed mineralization method for producing biomimetic structural materials, we introduce nanoparticles with different inherent functions into the platelets of artificial nacre via the co-mineralization of aragonite and the nanoparticles. Besides their enhanced mechanical properties, the obtained artificial nacre materials also exhibit different functions depending on the type of the nanoparticles. To extend the versatility of this strategy, the effects of nanoparticles of different sizes and zeta potentials on mineralization are also analyzed. This universal strategy can be applied to the fabrication of other types of functionalized biomimetic structural ceramics that have potential applications in various fields, such as biomedical science.

Keywords: artificial nacre; functionalize; nanoparticle; matrix-directed mineralization

CLC number: TB383 **Document code:** A

1 Introduction

Skeletal materials in biological systems, such as bones[1−3], teeth[4−6] and mollusk shells[7−9], provide mechanical support for living organisms to complete complex life functions. The remarkable performance of skeletal materials has been the focus of attention for several decades[10−12]. Many of these materials are essentially biological ceramics consisting of tiny minerals (e.g., calcium carbonate and hydroxyapatite) and ductile biopolymers connecting these tiny minerals. These tiny minerals and biopolymers are organized into complex hierarchical structures that enable the staggering mechanical performance of skeletal materials as well as other functions[10,13]. For example, nacre—the inner shell layer of some mollusks—consists of aragonite platelets and organic chitin interlayers, exhibiting a remarkably enhanced fracture toughness (40 times higher than that of pure aragonite)[9]. While it has been recognized that the upper limit of the mechanical performance of artificial ceramics can be extended by biomimetic structuralization, the fabrication of such hierarchically structured ceramics remains quite challenging[14−16]. Artificial structural ceramics with integrated multifunctions are highly desired as they can serve different purposes. By means of some fabrication methods such as freezing-casting[17−19], laminating[20,21], magnetically assisted slip-casting[22] and 3D printing[23], some of the structural features of nacre, e.g., the laminated structure, have been transcribed into artificial ceramics. However, their mechanical performance has yet to meet expectations, and multifunctional properties are absent in these materials[14]. These disadvantages are attributed to the following reasons. First, the structural features of artificial ceramics at a smaller scale have not been properly controlled, such as the occlusion of impurities inside the platelets. Second, it is difficult to homogeneously introduce guest nanoparticles with various functions into the host ceramics without disturbing the structure of the entire material[24]. In contrast, despite their low weight content, organic molecules and small ions as impurities in many biological ceramics are crucial to the performance of these materials[25,26]. Taking the above factors into consideration, we propose a facile fabrication strategy, i.e., biomimetic matrix-directed co-mineralization, to produce artificial nacre with both enhanced mechanical performance and multiple integrated functions.

2 Materials and methods

2.1 Materials

All raw materials and reagents were commercially available and used without further purification. Different sizes (10 nm, 25 nm, 80 nm, 150 nm, and 350 nm) of Fe_3O_4 nanoparticles (NPs) and polyacrylic acid (PAA, average M_w = 1800 g/mol) were purchased from Sigma-Aldrich Co. Chitosan (average

DOI: 10.52396/JUSTC-2022-0022
JUSTC, **2022**, 52(7): 1

M_w = 4800 g/mol), methanol, acetic anhydride, glacial acetic acid, Na_2CO_3, LiBr, $CaCO_3$, $MgCl_2$, $CdCl_2$, and $NaBH_4$ were purchased from Sinopharm Chemical Reagent. 3-Aminopropyltriethoxysilane was purchased from J&K Scientific. Mercaptopropionic acid and K_2TeO_3 were purchased from Aladdin Biochemical Technology Co., Ltd.

2.2 Synthesis

2.2.1 Laminated chitin matrix preparation

Chitosan (1 g) was dissolved in glacial acetic acid (GAA) solution (1 mL of GAA and 48 mL of deionized water (DIW)) followed by vigorous stirring. The obtained solution was treated according to the bidirectional freezing protocol in a polydimethylsiloxane mold. The frozen samples were subsequently dried in a Scientz-18N freeze-dryer (Ningbo Scientz Biotechnology Co., Ltd.) for 78 h. The obtained chitosan matrices were transformed into chitin matrices[17] in a mixed solution of methanol and acetic anhydride at 45 °C for 4.5 h. Then, the chitin matrices were washed several times with ethanol and water.

2.2.2 Silk fibroin (SF) sol preparation

SF sol was derived from *Bombyx mori* cocoons (Anhui Province, China) according to the protocol reported by Kaplan et al.[27]. Briefly, silkworm cocoons were treated with 0.02 mol/L of heated Na_2CO_3 solution to remove the gum. Then, the degummed fibers were dried and dissolved in 9.3 mol/L of LiBr solution (60 °C). The obtained transparent sol (SF sol) was dialyzed for 24 h to remove the residual ions.

2.2.3 Surface modification of Fe_3O_4 NPs

Commercially available negatively charged Fe_3O_4 NPs were treated to obtain positively charged Fe_3O_4 NPs. In a typical experiment, 1.0 g of Fe_3O_4 NPs were dispersed in 1000 mL of ethanol. Then, 2.21 g of 3-aminopropyltriethoxysilane was added to the mixture. The mixture was subjected to vigorous stirring overnight at 60 °C. The obtained positively charged Fe_3O_4 NPs were then separated and washed thoroughly with ethanol and DIW.

2.2.4 CdTe quantum dot synthesis

$CdCl_2$ (0.0533 g) was added to a three-necked flask with 50 mL of DIW followed by vigorous stirring. Then, 17.4 μL of mercaptopropionic acid was added to the solution at pH 10.5. Next, 0.01012 g of K_2TeO_3 powder was first dissolved in 50 mL of DIW by sonication for 5 min, and added to the solution at 100 °C followed by nitrogen gas bubbling. Finally, 0.0759 g of $NaBH_4$ was added. A series of CdTe quantum dots (QDs) with various fluorescent colors were obtained by heating the solution at 100 °C for 30 min, 2 h, and 5 h, respectively.

2.2.5 Mineralizing solution preparation

Excess calcium carbonate was mixed with DIW (2 L) at 25 °C followed by carbon dioxide gas bubbling. After 2 h, the solution was filtered to obtain a saturated calcium bicarbonate solution. PAA (0.6 mmol/L), $MgCl_2$ (24 mmol/L), and different concentrations of NPs, including magnetite NPs and CdTe QDs, were added to the calcium bicarbonate solution. The solutions with different NPs were used as the mineralizing solutions.

2.2.6 Fabrication of bulk artificial nacre

The predesigned chitin matrix was carefully placed in a silica rubber mold (12 mm × 12 mm × 15 mm). Then, 450 mL of mineralizing solution was pumped into the mold and flowed through the matrix repeatedly at 40 °C. The mineralizing solution was replaced twice (days 4 and 7); the entire mineralization process lasted for 12 days. Afterwards, the mineralized matrix was immersed in DIW for one day to remove residual salts and then dried in a Leica EM CPD300 supercritical drying system. The dried matrix was immersed in 0.4 wt% SF sol and then hot-pressed at 200 MPa in a steel mold (Fig. 1).

2.2.7 Characterization

Scanning electron microscopy (SEM) images were obtained with a Carl Zeiss Supra 40 field-emission scanning electron microscope at an acceleration of 3 kV. X-ray diffraction (XRD) patterns were obtained using a PANalytical X'pert PRO MRD X-ray diffractometer with CuKα1 radiation (λ = 1.54056 Å). Vickers hardness measurements were obtained using a microhardness tester (HX-1000, Suzhou AOKA Optical Instruments Co., Ltd.) with a maximum applied load of 0.3 kg for 10 s. Thermogravimetric analysis (TGA) data were acquired with a TA Instruments SDT Q600 thermogravimetric analyzer. Zeta potential data were obtained by a Zetasizer Nano S instrument (Malvern) at a pH of 6. The magnetic properties were acquired using a superconducting quantum interference device (SQUID, MPMS XL5). Photoluminescence (PL) spectra were collected using a Fluorolog-3-Tou

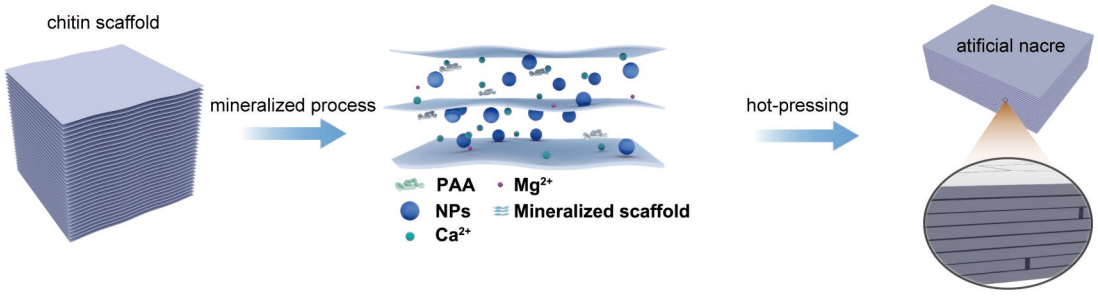

Fig. 1. Fabrication scheme of the artificial nacre.

DOI: 10.52396/JUSTC-2022-0022
JUSTC, **2022**, 52(7): 1

spectrometer (Jobin Yvon Inc.) at room temperature.

3 Results and discussion

3.1 Microstructures of the artificial nacre

Multifunctional nacre-mimetic ceramics are obtained through the co-mineralization method, where CdTe QDs and Fe_3O_4 NPs are incorporated into $CaCO_3$ mineral platelets (denoted as QDN and FeN, respectively) (Fig. 2). Aragonite is the only polymorph of $CaCO_3$ identified in both the QDN and FeN (Fig. 3a), which is precipitated under the control of Mg^{2+} and PAA[29,30]. The QDN exhibits steady-state PL upon excitation with 365 nm UV light (Fig. 3b). The PL wavelength of the QDN is slightly larger than that of the original QDs, which may be due to the slight shape distortion of the QDs in the aragonite platelets in the nacre[31,32]. The obtained FeN also exhibits ferromagnetism (Figs. 2c and 3c) owing to the incorporation of Fe_3O_4. These results indicate the inherent physical properties of the incorporated NPs (i.e., QDs and Fe_3O_4) are preserved even when they are co-mineralized with aragonite and embedded in the platelets. Both the QDN and FeN show a typical layered structure: the mineral layers are 1–4 μm with the thin polymer layers alternately distribute between the mineral layers. This structure is similar to that of the abalone nacre (Fig. 2d–f). Each mineral layer of the artificial nacre consists of microscale platelets that form distinct Voronoi patterns (Fig. 2g–i). The platelets (~ 40–300 μm) consist of aragonite nanograins and NPs. The sizes of the aragonite nanograins in both the QDN and FeN are approximately 10–100 nm (Fig. 2j–l). The nanograins in each platelet tend to orient randomly such that the entire platelet is polycrystalline. We suppose that the reorientation of the precipitated $CaCO_3$ nanograins, which can lead to the formation of a single crystal, is retarded by the high temperature and interaction between the host crystals and guest NPs[28]. By using the proposed matrix-directed co-mineralization strategy, different

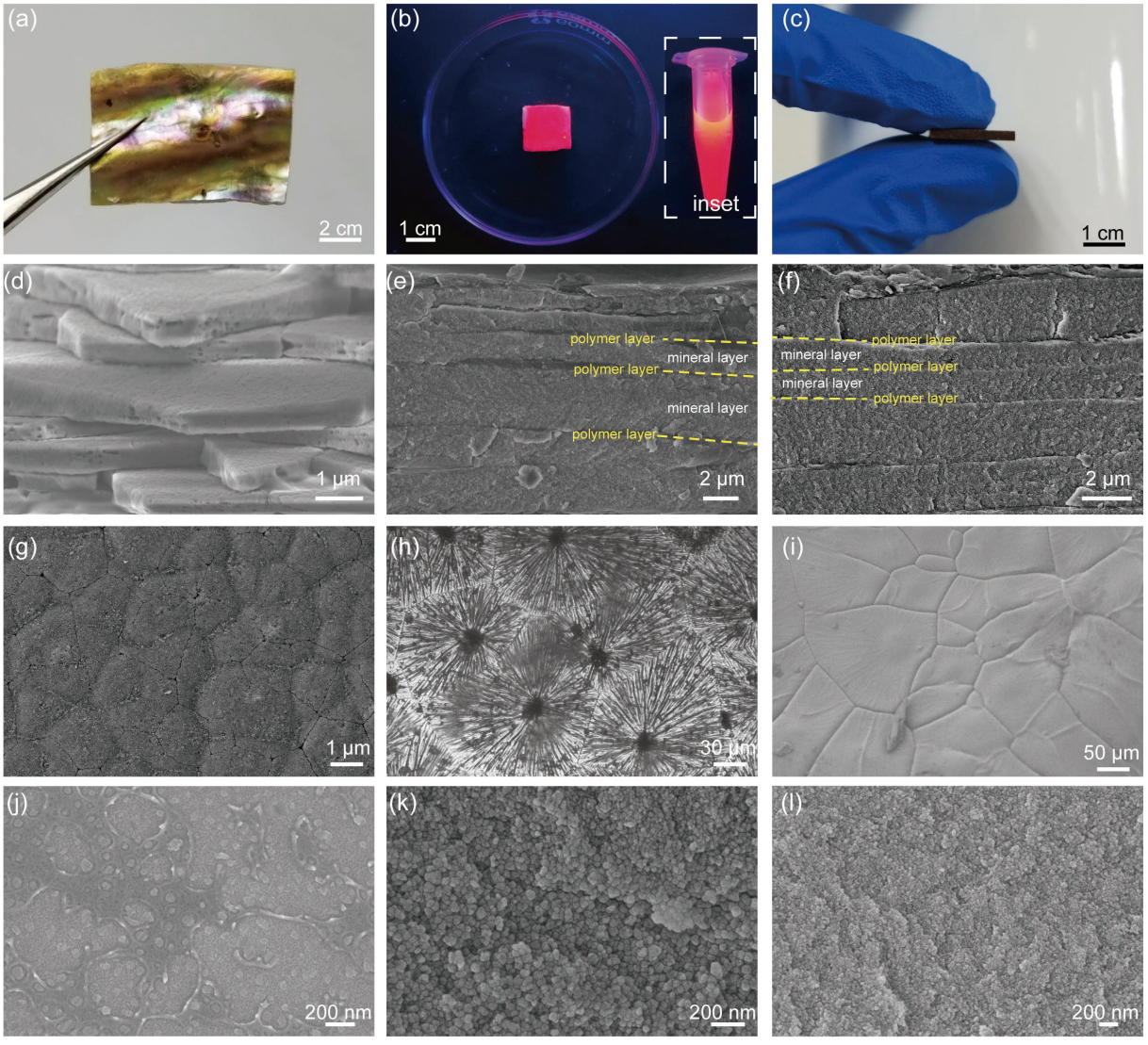

Fig. 2. Microstructure comparison between natural nacre and artificial nacre. (a) Abalone nacre. (b, c) Artificial nacre: (b) QDN and (c) FeN. The inset in (b) shows the PL of the original QDs. (d–f) Fracture surface of the (d) abalone nacre, (e) QDN, and (f) FeN. (g–i) Aragonitic layer of the (g) abalone nacre, (h) the QDN, and (i) FeN. (j–l) Enlarged micrographs of the aragonite platelets of the (j) abalone nacre, (k) QDN, and (l) FeN.

DOI: 10.52396/JUSTC-2022-0022
JUSTC, **2022**, 52(7): 1

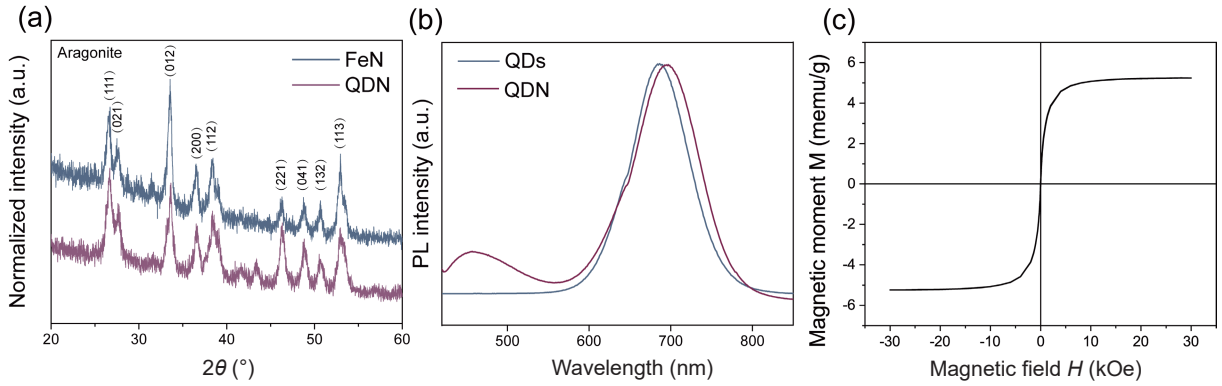

Fig. 3. Characteristics of the artificial nacre. (a) XRD patterns for the QDN and FeN. (b) Photoluminescence spectra of the QDN. (c) Magnetic hysteresis loops of the FeN.

functions are successfully introduced into the artificial materials while retaining their nacre-like structures.

3.2 The influence of the NPs properties on the artificial nacre

Because the properties of the NPs can strongly influence the precipitation of $CaCO_3$, we further studied the effects of the Fe_3O_4 NPs of various sizes and surface charges on the composition and structure of the artificial nacre (Fig. 4). Because the laminated structures of the matrices are the same despite the presence of different NPs, different artificial nacre samples obtained by the addition of different NPs all exhibit similar nacre-like laminated structure (Fig. 5). Analyses of the cross-sections of these artificial nacre samples reveal that negatively charged NPs are more easily embedded into the mineral hosts (Fig. 4). The chitin layers are mineralized into aragonite layers (Fig. 5a–f). In contrast, positively charged NPs can lead to a decrease in the aragonite content (Fig. 4). Some of the chitin membranes (yellow arrows in Fig. 5b, d, and f) remain unmineralized in the artificial nacre in the presence of positively charged NPs. While FeN_{10}− (i.e., the artificial nacre incorporated with ~ 10 nm negatively charged NPs) contains 92.8 wt% inorganic materials, FeN_{150}− and FeN_{350}− has much lower inorganic content (Fig. 4). These results reveal that aragonite precipitation onto the matrix is retarded by the increase in NP size (Fig. 4), which is also evidenced by

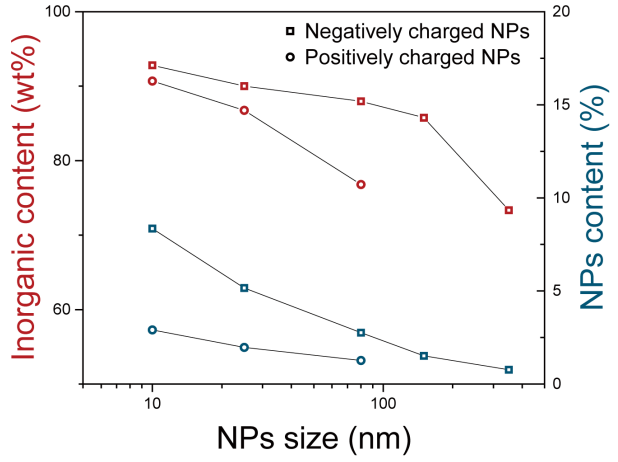

Fig. 4. Composition analysis of the artificial nacre with different NPs.

the significant amount of residual unmineralized chitin layers (Fig. 5g and h).

To understand the influence of the size and surface charge of NPs on the co-mineralization process, the morphological change of the Fe_3O_4 NPs in the solutions after 10 h is observed (Fig. 6). NPs with larger sizes are found to be more easily encapsulated by aragonite, which then grow even larger (Fig. 6a–e). Similarly, positively charged NPs are prone to coalesce with negatively charged polymer-stabilized aragonite and form large aggregates (Fig. 6f–h). The mobility as well as specific area of the NPs is restrained in both cases; consequently, the amount of incorporated NPs decreases. The large NP aggregates may also block mass transfer from the co-mineralization solution into some of the chitin layers; hence, that part of the matrix remains unmineralized (Fig. 5g and h), leading to a reduced inorganic content (Fig. 4). In contrast, the negatively charged Fe_3O_4 NPs with relatively small sizes are uniformly dispersed in the solution without aggregation (Fig. 6a). Thus, the mineralization process is carried out effectively, which contributes to the homogeneous mineralization of the entire matrix and the higher inorganic content of the artificial nacre (Figs. 4 and 5a).

3.3 Mechanical performance

Apart from the additional functions provided by the incorporated NPs, the NPs can also modify the mechanical behavior of the artificial nacre. The Vickers hardness values of the artificial nacre samples significantly varies (Fig. 7a). For example, while the Vickers hardness of FeN_{10}− can reach 183.5 ± 0.7 (HV0.3), that of FeN_{350}− is only 66.0 ± 2.6 (HV0.3), which is even lower than that of the artificial nacre without NP incorporation (NFN) (Fig. 7a). This can be attributed to the much lower inorganic content of the FeN_{350}− sample compared with the other NP-incorporated samples and NFN (Fig. 4). In general, the negatively charged NPs with smaller sizes can best enhance the Vickers hardness of the artificial nacre because both the inorganic material and incorporated NPs content can both be higher in this case (Fig. 4). The flexural stress of the artificial nacre is also influenced by NP incorporation. In particular, FeN_{10}− exhibits the highest flexural strength and modulus (Fig. 7b). This effect primarily stems from the inorganic composition and interactions

DOI: 10.52396/JUSTC-2022-0022
JUSTC, **2022**, 52(7): 1

between the NPs and aragonite[33]. The above data suggest that incorporating NPs with the proper size and surface charge[34,35] improves the mechanical performance of the obtained artificial nacre.

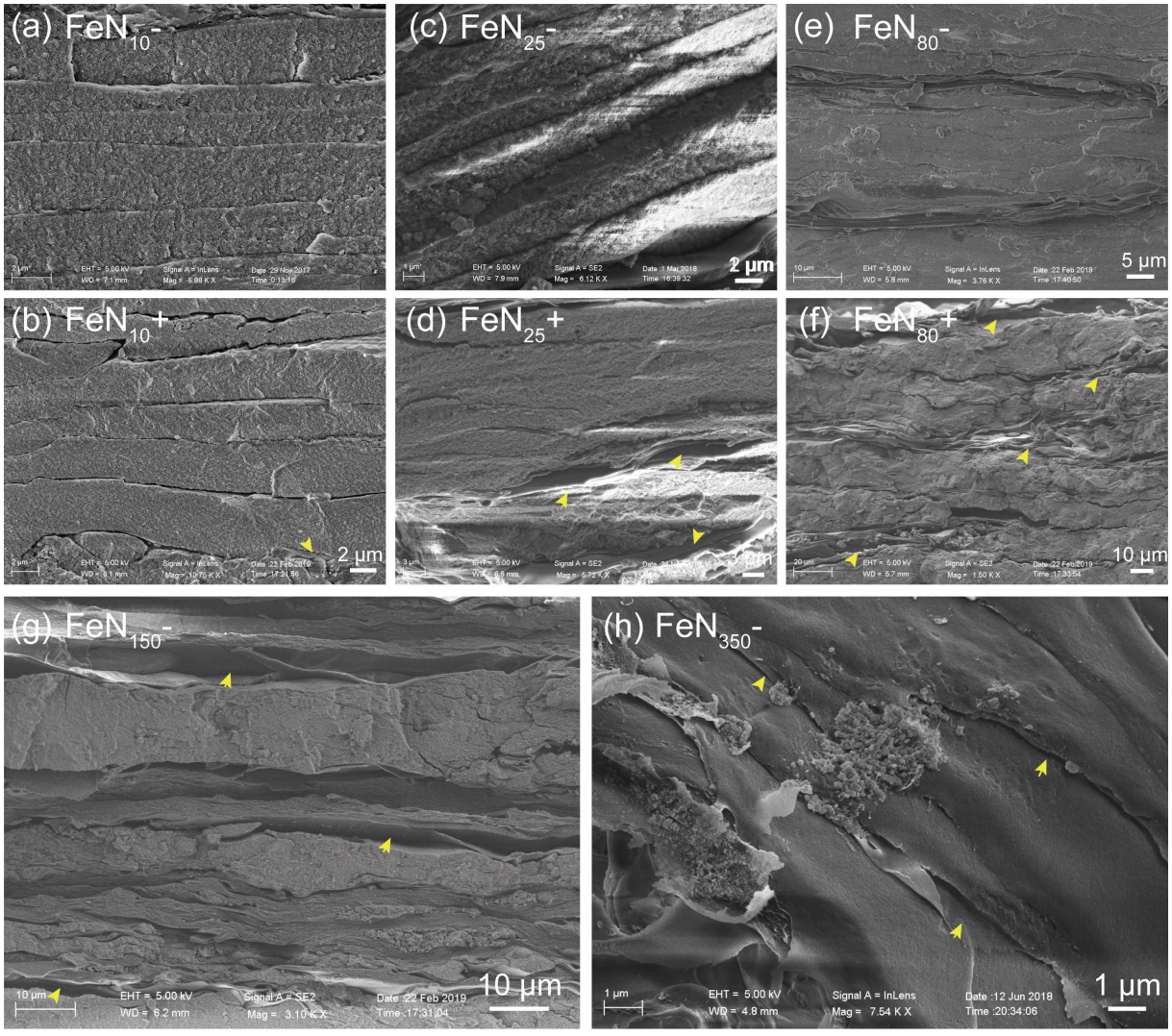

Fig. 5. Influence of the sizes and surface charges of the NPs on the microstructures of the artificial nacre. (a–h) Fracture surface of the artificial nacre: (a) FeN_{10}−, (b) FeN_{10}+, (c) FeN_{25}−, (d) FeN_{25}+, (e) FeN_{80}−, (f) FeN_{80}+, (g) FeN_{150}−, and (h) FeN_{350}−. FeN_{10}− is the artificial nacre incorporated with ~ 10 nm negatively charged NPs.

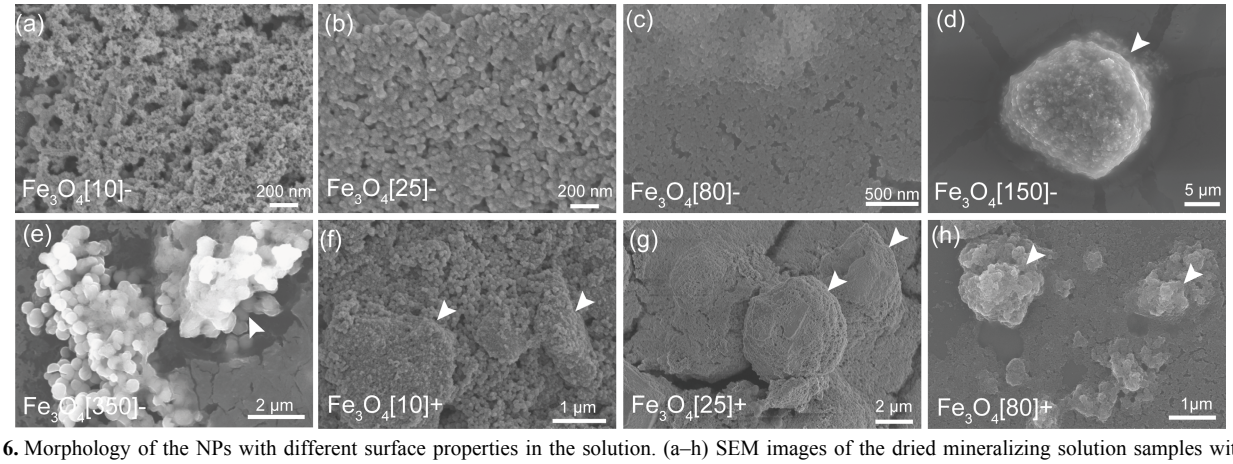

Fig. 6. Morphology of the NPs with different surface properties in the solution. (a–h) SEM images of the dried mineralizing solution samples with (a) Fe_3O_4[10]− NPs, (b) Fe_3O_4[25]− NPs, (c) Fe_3O_4[80]− NPs, (d) Fe_3O_4[150]− NPs, (e) Fe_3O_4[350]− NPs, (f) Fe_3O_4[10]+ NPs, (g) Fe_3O_4[25]+ NPs, and (h) Fe_3O_4[80]+ NPs. Fe_3O_4[10]− denotes the negatively charged Fe_3O_4 NPs with approximately 10 nm diameter.

DOI: 10.52396/JUSTC-2022-0022
JUSTC, **2022**, 52(7): 1

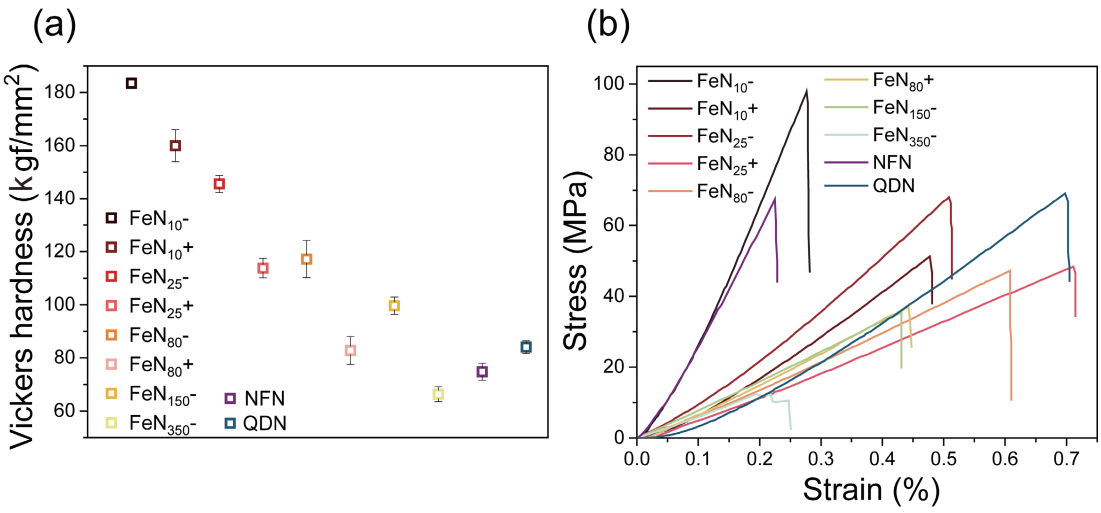

Fig. 7. Mechanical performance of artificial nacre: (a) Vickers hardness (at a load of HV0.3) and (b) flexural strength of different artificial nacre samples.

4 Conclusions

We have demonstrated that artificial nacre with multiple integrated functions and optimized mechanical performance can be obtained by the addition of different NPs with the appropriate size and surface charge during the mineralization of the matrix. The proposed matrix-directed co-mineralization strategy is a feasible and universal method to construct functionalized biomimetic materials. We anticipate that various artificial structural materials with different functions capable of meeting the demands of various applications can be fabricated.

Acknowledgements

This work was supported by the USTC Research Funds of the Double First-Class Initiative (YD2340002003) and Natural Science Foundation of Anhui Province (1808085ME114). This work was partially carried out at the USTC Center for Micro and Nanoscale Research and Fabrication.

Conflict of interest

The authors declare that they have no conflict of interest.

Biographies

Yu-Feng Meng received his Ph.D. degree in Inorganic Chemistry from University of Science and Technology of China in 2022. His research focuses mainly on biomimetic materials design.

Li-Bo Mao received his Ph.D. degree in Inorganic Chemistry from University of Science and Technology of China (USTC) in 2016. He is currently an assistant professor in the Hefei National Laboratory for Physical Sciences at the Microscale, USTC. His research focuses mainly on structure-property relationship of biological materials, preparation and application of biomimetic structural materials and biomineralization.

Shu-Hong Yu completed his Ph.D. in Inorganic Chemistry in 1998 from University of Science and Technology of China (USTC). He was appointed as a full professor in 2002 and the Cheung Kong Professorship in 2006 by the Ministry of Education in the Department of Chemistry, USTC. He was elected as an academician of Chinese Academy of Sciences in 2019. Currently, he is leading the Division of Nanomaterials & Chemistry, Hefei National Laboratory for Physical Sciences at the Microscale, USTC.

References

[1] Tertuliano O A, Greer, J R. The nanocomposite nature of bone drives its strength and damage resistance. *Nat. Mater.*, **2016**, *15* (11): 1195–1202.
[2] Reznikov N, Bilton M, Lari L, et al. Fractal-like hierarchical organization of bone begins at the nanoscale. *Science,* **2018**, *360* (6388): eaao2189.
[3] Duer M, Veis A. Bone mineralization: Water brings order. *Nat. Mater.*, **2013**, *12* (12): 1081–1082.
[4] DeRocher K A, Smeets P J M, Goodge B H, et al. Chemical gradients in human enamel crystallites. *Nature,* **2020**, *583* (7814): 66–71.
[5] Gordon L M, Cohen M J, MacRenaris K W, et al. Amorphous intergranular phases control the properties of rodent tooth enamel. *Science,* **2015**, *347* (6223): 746–750.
[6] La Fontaine A, Zavgorodniy A, Liu H, et al. Atomic-scale compositional mapping reveals Mg-rich amorphous calcium phosphate in human dental enamel. *Sci. Adv.*, **2016**, *2* (9): e1601145.
[7] Li L, Ortiz C. Biological design for simultaneous optical transparency and mechanical robustness in the shell of placuna placenta. *Adv. Mater.*, **2013**, *25* (16): 2344–2350.
[8] Bayerlein B, Zaslansky P, Dauphin Y, et al. Self-similar mesostructure evolution of the growing mollusc shell reminiscent of thermodynamically driven grain growth. *Nat. Mater.*, **2014**, *13* (12): 1102–1107.
[9] Sun J, Bhushan B. Hierarchical structure and mechanical properties of nacre: A review. *RSC Adv.*, **2012**, *2* (20): 7617–7632.
[10] Liu Z, Meyers M A, Zhang Z, et al. Functional gradients and heterogeneities in biological materials: Design principles, functions, and bioinspired applications. *Prog. Mater. Sci.*, **2017**, *88*: 467–498.
[11] Eder M, Amini S, Fratzl P. Biological composites-complex structures for functional diversity. *Science,* **2018**, *362* (6414): 543–547.
[12] Quan H, Kisailus D, Meyers M A. Hydration-induced reversible deformation of biological materials. *Nat. Rev. Mater.*, **2020**, *6* (3): 264–283.
[13] Amini S, Tadayon M, Idapalapati S, et al. The role of quasi-plasticity in the extreme contact damage tolerance of the stomatopod dactyl club. *Nat. Mater.*, **2015**, *14* (9): 943–950.
[14] Pro J W, Barthelat F. The fracture mechanics of biological and bioinspired materials. *MRS Bull.*, **2019**, *44* (1): 46–52.
[15] Wegst U G, Bai H, Saiz E, et al. Bioinspired structural materials.

DOI: 10.52396/JUSTC-2022-0022
JUSTC, **2022**, 52(7): 1

Nat. Mater., **2015**, *14* (1): 23–36.
[16] Ritchie R O. The conflicts between strength and toughness. *Nat. Mater.,* **2011**, *10* (11): 817–822.
[17] Mao L B, Gao H L, Yao H B, et al. Synthetic nacre by predesigned matrix-directed mineralization. *Science,* **2016**, *354*: 107–110.
[18] Munch E, Launey M E, Alsem D H, et al. Tough, bio-inspired hybrid materials. *Science,* **2008**, *322* (5907): 1516–1520.
[19] Bouville F, Maire E, Meille S, et al. Strong, tough and stiff bioinspired ceramics from brittle constituents. *Nat. Mater.,* **2014**, *13* (5): 508–514.
[20] Gao H L, Chen S M, Mao L B, et al. Mass production of bulk artificial nacre with excellent mechanical properties. *Nat. Commun.,* **2017**, *8* (1): 287.
[21] Yin Z, Hannard F, Barthelat F. Impact-resistant nacre-like transparent materials. *Science,* **2019**, *364* (6447): 1260–1263.
[22] Le Ferrand H, Bouville F, Niebel T P, et al. Magnetically assisted slip casting of bioinspired heterogeneous composites. *Nat. Mater.,* **2015**, *14*: 1172–1179.
[23] Torres A M, Trikanad A A, Aubin C A, et al. Bone-inspired microarchitectures achieve enhanced fatigue life. *Proc. Natl. Acad. Sci. U. S. A.,* **2019**, *116* (49): 24457–24462.
[24] Kim Y Y, Ganesan K, Yang P, et al. An artificial biomineral formed by incorporation of copolymer micelles in calcite crystals. *Nat. Mater.,* **2011**, *10* (11): 890–896.
[25] Pokroy B, Quintana J P, Caspi E N, et al. Anisotropic lattice distortions in biogenic aragonite. *Nat. Mater.,* **2004**, *3* (12): 900–902.
[26] Polishchuk I, Bracha A A, Bloch L, et al. Coherently aligned nanoparticles within a biogenic single crystal: A biological prestressing strategy. *Science,* **2017**, *358* (6368): 1294–1298.
[27] Rockwood D N, Preda R C, Yucel T, et al. Materials fabrication from *Bombyx mori* silk fibroin. *Nat. Protoc.,* **2011**, *6* (10): 1612–1631.
[28] Lloyd J A, Ng S H, Davis T J, et al. Size selective adsorption of gold nanoparticles by electrostatic assembly. *J. Phys. Chem. C,* **2017**, *121* (4): 2437–2443.
[29] Ichikawa R, Kajiyama S, Iimura M, et al. Tuning the *c*-axis orientation of calcium phosphate hybrid thin films using polymer templates. *Langmuir,* **2019**, *35* (11): 4077–4084.
[30] Xu J, Yan C, Zhang F, et al. Testing the cation-hydration effect on the crystallization of Ca-Mg-CO_3 systems. *Proc. Natl. Acad. Sci. U. S. A.,* **2013**, *110* (44): 17750–17755.
[31] Kim Y Y, Ganesan K, Yang P, et al. An artificial biomineral formed by incorporation of copolymer micelles in calcite crystals. *Nat. Mater.,* **2011**, *10* (11): 890–896.
[32] Huang W Q, Huang Z M, Cheng H Q, et al. Electronic states and curved surface effect of silicon quantum dots. *Appl. Phys. Lett.,* **2012**, *101* (17): 171601.
[33] Meng Y F, Zhu Y B, Zhou L C, et al. Artificial nacre with high toughness amplification factor: Residual stress-engineering sparks enhanced extrinsic toughening mechanisms. *Adv. Mater.,* **2021**, *34*: 2108267.
[34] Kulak A N, Semsarilar M, Kim Y Y, et al. One-pot synthesis of an inorganic heterostructure: Uniform occlusion of magnetite nanoparticles within calcite single crystals. *Chem. Sci.,* **2014**, *5* (2): 738–743.
[35] Kim Y Y, Darkins R, Broad A, et al. Hydroxyl-rich macromolecules enable the bio-inspired synthesis of single crystal nanocomposites. *Nat. Commun.,* **2019**, *10* (1): 5682.

DOI: 10.52396/JUSTC-2022-0022
JUSTC, **2022**, 52(7): 1